![JNeurosci: THE JOURNAL OF NEUROSCIENCE]

Dissociable Decoding of Spatial Attention and Working Memory from EEG Oscillations and Sustained Potentials

Gi-Yeul Bae and Steven J. Luck

Center for Mind & Brain and Department of Psychology, University of California — Davis, Davis, CA, 95618

Author contributions: G.-Y.B. and S.J.L. designed research; G.-Y.B. performed research; G.-Y.B. analyzed data; G.-Y.B. and S.J.L. wrote the paper.

Correspondence should be addressed to Address for correspondence: Gi-Yeul Bae, Ph.D, Center for Mind & Brain, University of California, Davis, 267 Cousteau Pl., Davis, CA 95618, (M) 410-491-5540, (E) gybae@ucdavis.edu

Alerts: Sign up at www.jneurosci.org/cgi/alerts to receive customized email alerts when the fully formatted version of this article is published.

1
2
3
4

**Dissociable Decoding of Spatial Attention and Working Memory from EEG
Oscillations and Sustained Potentials**

Gi-Yeul Bae and Steven J. Luck

Center for Mind & Brain and Department of Psychology
University of California – Davis
Davis, CA, 95618

Address for correspondence:

Gi-Yeul Bae, Ph.D.
Center for Mind & Brain
University of California, Davis
267 Cousteau Pl.
Davis, CA 95618
(M) 410-491-5540
(E) gybae@ucdavis.edu

Abbreviated title: Decoding of Working Memory
Number of figures: 9
Number of words: Abstract (200), Introduction (650), and Discussion (1,496)
Conflict of Interest: The authors declare no competing financial interests.

40   **Abstract**

41   In human scalp EEG recordings, both sustained potentials and alpha-band oscillations are present

42   during the delay period of working memory tasks and may therefore reflect the representation of

43   information in working memory. However, these signals may instead reflect support mechanisms

44   rather than the actual contents of memory. In particular, alpha-band oscillations have been tightly

45   tied to spatial attention and may not reflect location-independent memory representations per se.

46   To determine how sustained and oscillating EEG signals are related to attention and working

47   memory, we attempted to decode which of 16 orientations was being held in working memory by

48   human observers (both women and men). We found that sustained EEG activity could be used to

49   decode the remembered orientation of a stimulus, even when the orientation of the stimulus

50   varied independently of its location. Alpha-band oscillations also carried clear information about

51   the location of the stimulus, but they provided little or no information about orientation

52   independently of location. Thus, sustained potentials contain information about the object

53   properties being maintained in working memory, consistent with previous evidence of a tight

54   link between these potentials and working memory capacity. In contrast, alpha-band oscillations

55   primarily carry location information, consistent with their link to spatial attention.

56

57   *Keywords:* Alpha, EEG, ERP, Orientation, Working Memory, Decoding

58

59   **Significance Statement**

60

61   Working memory plays a key role in cognition, and working memory is impaired in several

62   neurological and psychiatric disorders. Previous research has suggested that human scalp EEG

63   recordings contain signals that reflect the neural representation of information in working

64   memory. However, to conclude that a neural signal actually represents the object being

65   remembered, it is necessary to show that the signal contains fine-grained information about that

66   object. Here, we show that sustained voltages in human EEG recordings contain fine-grained

67   information about the orientation of an object being held in memory, consistent with a memory

68   storage signal.

69

70

71

72

73   **Introduction**

74   Working memory (WM) is fundamentally important in cognitive processing, and

75   substantial effort has been devoted to understanding the neural coding of WM representations.

76   Most research has focused on the persisting neural activity that is present during the delay period

77   of WM tasks (Miller and Desimone, 1991; Todd and Marois, 2004; Fukuda et al., 2015) (but see

78   Stokes, 2015; Rose et al., 2016). However, this delay-period activity could reflect support

79   processes rather than the actual memory representations, and showing that the content of the

80   memory can be decoded from a neural signal provides much stronger evidence that the signal

81   represents the memory itself (Postle, 2016).

82   New EEG-based decoding methods show promise for studying the neural coding of

83   human WM (LaRocque et al., 2013; Foster et al., 2016; Rose et al., 2016; Wolff et al., 2017).

84   These studies used the scalp distribution of EEG signals to decode or track the information being

85   held in WM. However, it is quite plausible that they were actually tracking the direction of

86   spatial attention. For example, the scalp distribution of alpha-band EEG activity during the delay

87   period of a spatial WM task was found to track which of eight locations was being remembered

88   (Foster et al., 2016), but alpha oscillations are closely linked with spatial attention (Worden et

89   al., 2000), and observers often maintain spatial attention on the to-be-remembered location in

90   spatial WM tasks (Awh et al., 1998; Awh et al., 2000). Indeed, Rihs et al. (2007) showed that the

91   scalp distribution of alpha-band activity varies systematically according to which of eight

92   different locations is being attended. Moreover, Foster et al. (in press) found that alpha-band

93   activity tracks shifts of spatial attention, and van Ede et al. (2017) found that alpha-band activity

94   tracks the location of the item that is currently most relevant in WM. In addition, LaRocque et al.

95   (2013) and Rose et al. (2016) used EEG oscillations to decode the attended stimulus *dimension*

96   in a WM task, but they did not attempt to decode the specific feature *value* being maintained in

97   WM. It is possible that sustained attention is actually the mechanism of WM maintenance (Awh

98   and Jonides, 2001), but this is currently an open question (Woodman et al., 2001; Johnson et al.,

99   2008; Chun et al., 2011; Ester et al., 2012; Gazzaley and Nobre, 2012; Tas et al., 2016).

100   Sustained potentials are also present in averaged ERP waveforms during the delay period

101   of visual WM tasks (Perez and Vogel, 2012). These sustained potentials are strongly tied to

102   individual and group differences in WM storage capacity (Vogel and Machizawa, 2004; Leonard

103   et al., 2012), but no prior research has determined whether these potentials represent the features

104   of the remembered objects.

105   Both ERPs and fMRI have been used to decode the contents of WM in orientation

106   memory tasks (Harrison and Tong, 2009; Serences et al., 2009; Ester et al., 2013; Wolff et al.,

107   2015; Wolff et al., 2017), but these tasks may have encouraged participants to focus attention on

108   the end of the oriented grating (see Fig. 1a), and it is possible that the direction of spatial

109   attention was being decoded rather than orientation per se (Fahrenfort et al., 2017). Thus, it is not

110   yet known whether EEG signals contain information about nonspatial features being maintained

111   in WM.

112   In the present study, we conducted two EEG decoding experiments, one using a simple

113   orientation task that could potentially be performed by means of either spatial attention or

114   location-independent orientation representations (or both), and one that can dissociate between

115   orientation and location. Given the close association between sustained ERP responses and WM

116   capacity (Vogel and Machizawa, 2004), we predicted that these responses would reflect the

117   specific feature value being maintained in WM. By contrast, given the close association between

118   alpha-band oscillations and attention (Worden et al., 2000; Rihs et al., 2007), we predicted that

119   these oscillations would reflect the location of the to-be-remembered object rather its features.

120   **Materials and Methods**

121   *Participants*

122   Sixteen college students between the ages of 18 and 30 with normal or corrected-to-

123   normal visual acuity participated in each experiment for monetary compensation (Experiment 1:

124   10 female, 6 male; Experiment 2: 9 female, 7 male). All participants had experience with at least

125   one prior WM task. The study was approved by the UC Davis Institutional Review Board.

126   *Stimuli & Apparatus*

127   Stimuli were generated in Matlab (The Mathworks, Inc.) using PsychToolbox (Brainard,

128   1997; Pelli, 1997) and were presented on an LCD monitor (Dell U2412M) with a gray

129   background (31.2 cd/m2) at viewing distance of 100 cm. A black fixation dot was continuously

130   present in the center of the display except during the intertrial interval, and participants were

131   instructed to maintain fixation on this dot except during the response period and intertrial

132   interval.

133   *Experiment 1 Behavioral Task*

134   We conducted two experiments using different behavioral tasks. Experiment 1 was

135   designed to establish our ability to decode the feature value being remembered using both alpha-

136   band and sustained ERPs in a simple task that could be performed either by means of spatial

137   attention or orientation memory (or both). Experiment 2 was designed to dissociate spatial

138   attention from orientation.

139   Experiment 1 used a standard delayed estimation task (Fig. 1b). Each trial started with a

140   500-ms presentation of the fixation dot followed by a 200-ms presentation of a black, teardrop-

141   shaped *sample stimulus* (2.17º long, 0.8° maximum width) that was centered on the fixation dot.

142   Sixteen discrete teardrop orientations were used (0°, 22.5°, 45°, 67.5°, 90°, 112.5°, 135°, 157.5°,

143   180°, 202.5°, 225°, 247.5°, 270°, 292.5°, 315°, and 337.5°), tested in random order with equal

144   probability. Participants were instructed to remember the orientation of this teardrop as precisely

145   as possible over a 1300-ms delay period during which only the fixation dot was visible. A

146   response ring (radius 2.17°) was then presented to indicate that a response should be made; once

147   the participant started moving the mouse to respond, a *test* teardrop appeared at the center of the

148   response ring. Participants were instructed to adjust the orientation of the test teardrop so that it

149   matched the remembered orientation of the sample teardrop. The test was identical to the sample,

150   except that its initial orientation was determined by the mouse pointer position when the

151   participant began to respond (and was therefore unrelated to the orientation of the sample

152   teardrop). The orientation of the test teardrop was continuously updated while the mouse moved

153   so that the tip of teardrop always pointed toward the current mouse pointer position. This made

154   the tip of the teardrop highly salient. Once participants were satisfied with the orientation, they

155   finalized the report by clicking a mouse button. The display then blanked completely, and the

156   next trial started after a 1000-ms delay. Note that participants could potentially perform this task

157   by focusing spatial attention onto the location of the sample teardrop's tip during the delay

158   period and then adjusting the test teardrop until it's tip was at the attended location, without

159   remembering the orientation of the teardrop per se. Even if they did not use this as the sole

160   memory strategy, they may have focused attention on the remembered location of the teardrop

161   during the delay period as they prepared to make their response.

162   Each participant completed a total of 640 trials (40 trials for each of the 16 orientations,

163   in random order). Each participant received at least 16 practice trials before beginning the task.

164   Note that the teardrop-shaped stimuli used in this study provide 360° of distinct

165   orientations, whereas other classes of commonly used orientation stimuli (e.g., Gabor patches)

166   can produce only 180° of distinct orientations. In mathematical terms, the present stimuli can be

167   described in terms of the orientation of a *ray*, whereas stimuli such as Gabor patches can be

168   described in terms of the orientation of a *line* (of infinite length).

169   *Experiment 2 Behavioral Task*

170   The task in Experiment 2 (Fig. 4) was designed to completely dissociate the orientation

171   of the teardrop from its location, making it possible to determine whether a given neural signal

172   contains information about location or about orientation (or both). It was identical to the delayed

173   estimation task used in Experiment 1, except that the location of the sample and test teardrops

174   varied independently from trial to trial. Thus, the location of the tip of the sample teardrop

175   provided no information about the orientation of the teardrop.

176   We assumed that attention would be directed to the location of the sample teardrop when

177   it was being perceived and encoded, but the stimuli were designed so that maintaining attention

178   on this location would not allow participants to report the teardrop orientation at the time of test.

179   In addition, this procedure allowed us to independently decode both the location and the

180   orientation of the sample teardrop. We predicted that alpha-band activity could be used to decode

181   the location but not the orientation of the teardrop, indicating that this signal primarily reflects

182   spatial attention. By contrast, we predicted that sustained EEG voltages could be used to decode

183   the orientation of the teardrop, indicating that this signal reflects a location-independent WM

184   representation. There are multiple ERP components that track the location being attended (N2pc

185   and sustained posterior contralateral negativity — Jolicoeur et al., 2008; Luck, 2012; Fahrenfort

186   et al., 2017), so we assumed that we would be able to decode the location of the teardrop as well

187   as its orientation from the ERP signals.

188   The orientation of a given teardrop was defined by the angular position of the tip relative

189   to the center of the object itself (Fig. 4b, θ_O). As in Experiment 1, 16 discrete orientations were

190   possible (0°, 22.5°, 45°, 67.5°, 90°, 112.5°, 135°, 157.5°, 180°, 202.5°, 225°, 247.5°, 270°,

191   292.5°, 315°, and 337.5°). The tip of the sample teardrop was always located at one of 16

192   discrete locations (0°, 22.5°, 45°, 67.5°, 90°, 112.5°, 135°, 157.5°, 180°, 202.5°, 225°, 247.5°,

193   270°, 292.5°, 315°, and 337.5°) on an invisible circle with a radius of 2.17° that was centered on

194   the fixation dot. Its location was defined by the angular position of the tip relative to the center of

195   this invisible circle (Fig. 4b, θ_L). The location and orientation of the sample teardrop on a given

196   trial were chosen at random from the 256 possible combinations of the 16 orientations and 16 tip

197   locations so that the orientation and location were completely independent (Fig. 4c). For

198   example, the tip of a teardrop with a 45° orientation could be placed at any of the 16 locations.

199   Similarly, a teardrop with a tip located at 292.5° could have any of the 16 orientations. The only

200   constraint was that each of the 16 orientations and each of the 16 locations occurred on the same

201   number of trials (but selected independently of each other). Consequently, remembering the

202   location of the teardrop would not help in reporting its orientation. Participants were told nothing

203   about the constraints on the orientation and location of the teardrop; they were simply told that

204   the locations of the sample and test teardrops would differ and that they should adjust the

205   orientation of the test teardrop so that it matched the orientation of the sample.

206   Orientation cannot be completely dissociated from location because orientation is defined

207   by a pattern of change over space. In the present experiment, teardrop orientation can therefore

208   be defined as the location of the tip of the teardrop relative to the center or thick end of the

209   teardrop. Thus, the contrast between stimulus orientation and stimulus location can be

210   equivalently framed as a difference between an object-centered spatial representation

211   (orientation) and an environment-centered (or retinotopic) spatial representation (which is a

212   fundamental issue in visual coding — Bisiach, 1996). For the sake of simplicity, however, the

213   present paper uses the term *orientation* to mean an object-centered representation and the terms

214   *location* and *space* to refer to an environment-centered or retinotopic representation.

215   In orthogonalizing the location and orientation of the teardrop, we focused on the

216   teardrop's tip because it was the part of the teardrop that provided the most precise location

217   information and because the tip always pointed toward the location of the mouse pointer while

218   the participant was attempting to reproduce the sample orientation, making it highly salient. In

219   theory, the location of the thick end of the teardrop could provide some information about the

220   teardrop's orientation in this task, but a later section will provide evidence that this could not

221   have influenced our orientation decoding results.

222   The location of the test teardrop was determined by a new random combination of

223   orientation and location, selected at random on each trial, independently of the orientation and

224   the location of the sample teardrop on that trial. In other words, the test teardrop was selected at

225   random from among the same set of 256 possibilities as the sample teardrop. However, when the

226   observer rotated the teardrop, its tip was no longer constrained to fall on the invisible circle used

227   to define the sample teardrop locations. Consequently, participants could not use the location of

228   the test teardrop to guess the orientation of the sample teardrop. In addition, this task makes it

229   possible to determine whether a decoder that is trained with orientations at one set of locations

230   can decode orientations presented at a different set of locations.

231   After at least 16 practice trials, each participant completed a total of 640 trials (40 for

232   each of the 16 orientations, collapsed across location, which was also 40 for each of the 16

233   locations, collapsed across orientation).

234   *EEG Recording & Preprocessing*

235   The continuous EEG was recorded using a Brain Products actiCHamp recording system

236   (Brain Products GmbH). Recordings were obtained from a broad set of scalp sites (FP1, FP2, F3,

237   F4, F7, F8, C3, C4, P3, P4, P5, P6, P7, P8, P9, P10, PO3, PO4, PO7, PO8, O1, O2, Fz, Cz, Pz,

238   POz, and Oz), which was similar to the montage used in the spatial WM study of Foster et al.

239   (2016). Electrodes on the left and right mastoids were recorded for use as reference sites. The

240   horizontal electrooculogram (EOG) was recorded from electrodes placed lateral to the external

241   canthi and was used to detect horizontal eye movements; the vertical EOG was recorded from an

242   electrode placed below the right eye and was used to detect eyeblinks and vertical eye

243   movements. Electrode impedances were maintained below 50 KΩ. All signals were recorded

244   single-ended and then referenced offline. The EEG was filtered online with a cascaded

245   integrator-comb antialiasing filter (half-power cutoff at 130 Hz) and digitized at 500 Hz.

246   Signal processing and analysis was performed in Matlab using EEGLAB Toolbox

247   (Delorme and Makeig, 2004) and ERPLAB Toolbox (Lopez-Calderon and Luck, 2014). The

248   scalp EEG was referenced offline to the average of the left and right mastoids. A bipolar

249   horizontal EOG derivation was computed as the difference between the two horizontal EOG

250   electrodes, and a vertical EOG derivation was computed as the difference between Fp2 and the

251   electrode below the right eye. All the signals were band-pass filtered (non-causal Butterworth

252   impulse response function, half-amplitude cut-offs at 0.1 and 80 Hz, 12 dB/oct roll-off) and

253   resampled at 250 Hz. Portions of EEG containing large muscle artifacts or extreme voltage

254   offsets (identified by visual inspection) were removed. Independent component analysis (ICA)

255   was then performed on the scalp EEG for each subject to identify and remove components that

256   were associated with blinks (Jung et al., 2000) and eye movements (Drisdelle et al., 2017). The

257   ICA-corrected EEG data were segmented for each trial from -500 to +1500 ms relative to the

258   onset of the sample teardrop. To verify that eye movements did not impact the decoding results,

259   we also conducted a set of decoding analyses in which trials with eye movements were excluded

260   and ICA-based correction was not applied (see below).

261   *Decoding Overview*

262   We attempted to decode the orientation of the sample stimulus based on the scalp

263   distribution of two different signals, the phase-independent alpha-band EEG power and the

264   phase-locked ERP voltage. To ensure that we were decoding non-overlapping signals in these

265   two analyses, the ERP decoding procedure was limited to frequencies below 6 Hz, and the alpha-

266   band decoding procedure was limited to frequencies between 8 and 12 Hz. Thus, we could be

267   certain that the ERP decoding was not contaminated by alpha-band oscillations, which can

268   masquerade as sustained ERPs under some conditions (Mazaheri and Jensen, 2008; van Dijk et

269   al., 2010), and we could also be certain that the alpha-band decoding was not contaminated by

270   low-frequency sustained potentials. Decoding was performed independently at each time point,

271   but the statistical analysis focused on temporally contiguous clusters of above-chance decoding

272   performance.

273   There are many ways to assess the relationship between a stimulus parameter such as

274   orientation and a neural signal, but the most common approaches are forward encoding models

275   and decoding procedures (Serences et al., 2009; Brouwer and Heeger, 2011; Foster et al., 2016;

276   Fahrenfort et al., 2017). Here, we chose to focus on decoding because the goal was to determine

277 whether the signals contain information about the orientation of the sample stimulus, and above-

278 chance decoding accuracy provides the most straightforward evidence that such information is

279 present. Forward encoding models can be very valuable, but they make assumptions about the

280 nature of the underlying representation that may not be justified for a given feature dimension

281 and are not relevant to the questions being asked in the present study. Although we report only

282 the decoding approach here, we have also applied the forward encoding approach (using the

283 method of Foster et al., 2016), which yielded a comparable pattern of results.

284   As in other EEG decoding/encoding studies (Foster et al., 2016, in press), the data from a

285 given orientation were averaged across multiple trials to improve the signal-to-noise ratio (after

286 extracting the phase-independent alpha power or the low-frequency EEG signals), and decoding

287 was performed on these averages rather than on single-trial data. A separate classifier was

288 trained to discriminate between each orientation (after averaging across trials) and all the other

289 orientations. Decoding accuracy was then computed for the average of a set of trials for each

290 orientation that was left out of the training data. Decoding was considered correct only if the

291 classifier correctly determined which one of the 16 orientations was being held in WM. Chance

292 performance was therefore 6.25% (1/16).

293   We focused our oscillatory power analyses on the alpha band, which is the frequency that

294 exhibited the most consistent relationship with WM in previous EEG research (Foster et al.,

295 2016). We also conducted exploratory analyses of a broad range of frequencies (4 Hz bands

296 between 4 and 48 Hz). Some weak decoding was observed in the low beta range (12-16 Hz), but

297 no clear decoding was present beyond the initial stimulus encoding period in any other band, so

298 the present paper will focus only on the alpha band.

299   *Experiment 1 Decoding Analysis*

300   The decoding procedure for Experiment 1 was the same for the alpha-band signals and

301   the low-frequency ERP signals, except for the initial steps used to isolate the signal of interest.

302   For the alpha-band decoding, the segmented EEG was bandpass filtered at 8-12 Hz using the

303   EEGLAB eegfilt() routine, which implements a two-way least-squares finite impulse response

304   filter with maximally steep rolloffs and an extremely narrow transition band. The bandpass

305   filtered EEG segments were then submitted to a Hilbert transform to compute the magnitude of

306   the complex analytic signal, and this magnitude was then squared to compute total power in the

307   8-12 Hz band at each time point. For the ERP decoding, the segmented EEG was simply low-

308   pass filtered at 6 Hz, again using the EEGLAB eegfilt() routine. In both cases, the data were then

309   resampled at 50 Hz (one data point per 20 ms) to increase the efficiency of the analyses. For each

310   of the two signals, this gave us a 4-dimensional data matrix for each participant, with dimensions

311   of time (100 time points), orientation (16 different values), trial (40 individual trials for each

312   orientation), and electrode site (the 27 scalp sites).

313   We used the combination of a support vector machine (SVM) and error-correcting output

314   codes (ECOC — Dietterich and Bakiri, 1995) to classify the orientation of the sample teardrop

315   on the basis of the spatial distribution of the signal over the 27 scalp electrodes. The ECOC

316   model solves multiclass categorization problems by combining results from multiple binary

317   classifiers. This model was implemented through the Matlab fitcecoc() function. The data were

318   decoded separately for each of the 100 time points from -500 ms to +1480 ms (relative to sample

319   array onset). However, our statistical analyses focused only on the delay interval (the 1300-ms

320   period beginning at the offset of the sample teardrop and continuing through the last sample

321   before the onset of the test teardrop).

322   The decoding for a given time point had separate training and test phases. In the training

323   phase, 16 different SVMs were trained, one for each orientation. A one-versus-all approach was

324   taken, in which each SVM was trained to distinguish between one specific orientation and all the

325   other orientations. In the test phase, new data from each of the 16 orientations was fed into all 16

326   SVMs, and the set of orientation assignments that minimized the average binary loss across the

327   set of 16 SVMs was selected (see below). This procedure was used to classify the test data for

328   each of the 16 orientations.

329   Separate trials were used for training and testing. Specifically, the decoding for each time

330   point used a 3-fold cross-validation procedure in which the data from 2/3 of the trials (selected at

331   random) were used to train the classifier, and then the performance of the classifier was assessed

332   with the data from the remaining 1/3 of trials. As a first step, we organized the data with respect

333   to teardrop orientation and then divided the trials into three equal sized groups of trials (three

334   groups of 13 trials for each of the 16 orientations). One random trial from each of the 16

335   orientations was omitted because 40 is not evenly divisible by 3. The trials for a given

336   orientation in each group were averaged together, producing a scalp distribution for the time

337   point being analyzed (a matrix of 3 groups x 16 orientations x 27 electrodes). The data from two

338   of the three groups served as a training dataset, and the remaining group served as a testing

339   dataset. The two training datasets were simultaneously submitted to the ECOC model with

340   known orientation labels to train the 16 SVMs. Each SVM learned to perform a binary

341   classification that separated one of the 16 orientations from the other 15 orientations at the

342   current time point.

343   Next, the set of 16 trained ECOC models was used to predict which of the 16 orientations

344   was present for each of the unlabeled orientations in the group of data that were reserved for

345   testing. This was done with the Matlab predict() function. This function assigns a class label for

346   each observation in the testing dataset by minimizing the average binary loss over the 16 SVMs.

347   The output of this function provides one predicted orientation for each of the 16 orientations in

348   the testing dataset. Decoding accuracy was then computed by comparing the true orientation

349   labels with the predicted labels. To be considered correct, we required that the predicted

350   orientation exactly match the true orientation, providing a very stringent assessment of decoding.

351   We have conducted additional analyses examining "near misses", but those analyses are beyond

352   the scope of this paper.

353   This procedure was repeated three times, once with each group of data serving as the

354   testing dataset. To minimize idiosyncrasies associated with the assignment of trials to groups, we

355   iterated the entire procedure 10 times with new random assignments of trials to the three groups.

356   After completing all the iterations of the cross-validation procedure, decoding accuracy was

357   collapsed across the 16 orientations, across the three cross-validations, and across the 10

358   iterations, producing a decoding percentage for a given time point that was based on 480

359   decoding attempts (16 orientations x 3 cross validations x 10 iterations). After this procedure was

360   applied to each time point, the averaged decoding accuracy values were smoothed across time

361   points to minimize noise using a 5-point moving window (equivalent to a time window of ±40

362   ms).

363   The temporal precision resulting from the entire EEG processing and decoding pipeline

364   was approximately ±50 ms. This was determined by running a 600-ms boxcar function through

365   the portions of the pipeline that produced low-pass filtering (including the final smoothing step),

366   which produced a temporally smeared version of the boxcar function. The point at which this

367   function reached 10% of the maximum voltage was approximately 50 ms before the beginning

368   and 50 ms after the end of the original boxcar function. Small ripples extended further in time

369   but were less than 10% of the original signal size.

370   *Statistical analysis of decoding accuracy*

371   If the pattern of voltage over the 27 electrodes contains information about the stimulus

372   orientation, then decoding accuracy should be greater than chance, which was 1/16 because we

373   used 16 teardrop orientations. To compare decoding accuracy to chance at each time point while

374   controlling for multiple comparisons, we used a nonparametric cluster-based Monte Carlo

375   simulation technique that is analogous to the cluster-based mass univariate approach that is

376   commonly used in EEG research (Maris and Oostenveld, 2007; Groppe et al., 2011). This

377   method is useful here both because it provides an intelligent correction for multiple comparisons

378   and because decoding accuracy may not be normally distributed. This method involved three

379   main steps.

380   In Step 1, we tested whether the obtained decoding accuracy at each individual time point

381   during the 1300-ms delay interval was greater than chance using one-sample t-tests comparing

382   the mean accuracy across participants to chance (1/16). We used one-tailed tests because the

383   SVM approach could not produce meaningful below-chance decoding. Note that this excluded

384   the first 200 ms following stimulus onset to minimize the contribution of sensory activity to the

385   decoding and focus on signals related to working memory. We then found clusters of contiguous

386   time points for which the single-point *t* tests were significant ($p < .05$), and the *t* scores within

387   each such cluster were then summed together to produce a cluster-level *t* mass. Each cluster-

388   level *t* mass was then compared against a null distribution for the cluster-level *t* mass that was

389   determined via Monte Carlo simulations in Step 3. In other words, we asked whether the mass of

390   a cluster of contiguous, individually significant *t* values was greater than the mass that would be

391   expected by chance. This controls the Type I error rate at the cluster level, yielding a probability

392   of .05 that one or more clusters would be significant if true decoding accuracy were at chance

393   during the entire delay period (Groppe et al., 2011).

394   In Step 2, we constructed a Monte Carlo null distribution of cluster-level t mass values.

395   To accomplish this, we first simulated the decoding accuracy that would be obtained if the

396   decoder randomly guessed the orientation of the stimulus with no knowledge of the actual

397   orientation. On each simulated trial, we randomly sampled an integer between 1 and 16 as the

398   response of the decoder for a given target orientation. The response was scored as correct if it

399   was the same as the target value. This was repeated 480 times (16 target orientations x 3 cross-

400   validations x 10 iterations), and the 480 scores were aggregated to compute the mean simulated

401   decoding accuracy at a given time point. This procedure was repeated independently for each of

402   the 100 time points, just as we independently decoded the EEG data at each time point. The

403   resulting series of decoding accuracy values was then smoothed with a 5-point running average

404   filter. This is the same procedure that was used to quantify the actual SVM decoding accuracy

405   for a given participant, but using a random decoder instead of the SVM-based decoder. This

406   procedure was then repeated 16 times to represent each of our 16 participants.

407   We then used these simulated decoding accuracy values to compute the cluster-level t

408   mass using the same procedure described in Step 1 (limited to the time points during the 1300-

409   ms delay period). If there were no significant t values, the cluster mass was zero. If there was

410   more than one cluster of individually significant t values, we took the mass of the largest cluster.

411   This simulated the maximum t mass from a single experiment in which decoding was at chance.

412   In Step 3, we obtained a null distribution for the cluster mass. This involved simulating a

413   large number of experiments in which the null hypothesis is true (i.e., decoding is at chance) and

414   examining the probability of getting a given maximum cluster mass across these simulated

415   experiments. Specifically, we conducted 10,000 iterations of the procedure from Step 2, making

416   it possible to construct the null distribution of the maximum cluster-level t mass (with a

417   resolution of $p = 10^{-4}$). We then computed the p value corresponding to each cluster in the actual

418   data set by examining where each observed t mass fell within the null distribution. The p value

419   for a given cluster was set based on the nearest percentiles of the null distribution (using linear

420   interpolation). If the obtained cluster-level t mass is larger than the maximum of simulated

421   cluster-level t mass, then we reported $p < 10^{-4}$. We rejected the null hypothesis and concluded

422   that the decoding was above chance for any observed cluster-level t mass that was in the top 95%

423   of the null distribution (critical t mass = 12.0717, one-tailed, alpha = .05). Note that this analysis

424   was limited to the 1300-ms delay period because the goal was to test decoding accuracy during

425   working memory maintenance.

426   *Experiment 2 Decoding Analysis*

427   The decoding procedure for Experiment 2 was identical to that for Experiment 1, with the

428   following exceptions. First, we independently decoded the orientation of the teardrop and the

429   location of the teardrop's tip. We collapsed across tip locations when we decoded the orientation,

430   and we collapsed across orientations when we decoded the tip location. Because orientation and

431   tip location were completely counterbalanced, the decoding of orientation could not have been

432   influenced by information about tip location, and vice versa.

433   In addition to the main statistical testing, we also compared decoding accuracy for

434   location versus orientation. We used the same cluster mass approach, but with two differences.

435   First, we used two-tailed t tests because either feature could conceivably produce more accurate

436   decoding. Second, the Monte Carlo null distribution was constructed by randomly swapping

437 labels for the two conditions being compared, matching the procedure used to compare cluster

438 masses for two waveforms in EEG experiments (Groppe et al., 2011). The null distribution

439 constructed by this method represents the probability distribution of the t mass under the

440 assumption that the obtained decoding accuracy for the two conditions are just different

441 instances sampled from the same distribution. We computed the p value corresponding to each

442 cluster in the actual data set by examining where each observed t mass fell within this null

443 distribution, and we rejected the null hypothesis if the observed t mass fell within the top or

444 bottom 2.5% of values from the null distribution (critical t mass = [-1.88, 2.73], two-tailed, alpha

445 = .05).

446   As noted earlier, we used the tip of the orientation for the counterbalancing because the

447 tip was the most informative part of the teardrop and was directly controlled by the mouse

448 pointer. However, one might be concerned that participants paid attention to some other part of

449 the teardrop, such as the thick end, causing a small but nonzero association between the

450 orientation of the teardrop and the location of some part of the teardrop. For example, the thick

451 end of the rightward-pointing teardrops was farther to the left, on average, than the thick end of

452 the leftward pointing teardrops (see Figure 4c). However, both the behavioral task and the

453 decoding algorithm required discriminating between one orientation and all other possible

454 orientations (i.e., not just leftward-vs-rightward). In addition, almost every location of the thick

455 end of the teardrop was associated with multiple orientations (with all possible combinations of

456 orientations across the possible locations). As a result, attending to the thick end of the teardrop

457 did not provide unique information about the orientation of the teardrop.

458   For these reasons, it is extremely unlikely that this location information could impact our

459 orientation decoding. To provide support for this assumption, we conducted both an additional

460   analysis and a simulation. In the additional analysis (described in the *cross-feature decoding*

461   section below), we trained the orientation decoder using teardrops presented at one set of

462   locations and then tested the decoder with data from teardrops that were presented at a different

463   set of locations. Above-chance level decoding in this analysis provides evidence that orientation

464   of teardrop can be decoded completely independently of location.

465   In addition, we conducted a simulation in which we attempted to decode teardrop

466   orientation on the basis of the location of the thick end of each teardrop using the exact X,Y

467   coordinates of this location (as if we had two electrodes, one that perfectly represented the X

468   value and one that perfectly represented the Y value corresponding to the thick end of the

469   teardrop). Note that the same thick end location can be occupied by multiple orientations and an

470   area of thick end locations of one orientation was occupied by thick end locations of other

471   orientations. As a result, the thick end locations for one orientation were not linearly separable

472   from the thick end locations of the other orientations in the two-dimensional space.

473   Consequently, to provide a stronger test of decodability, we used a non-linear SVMs with a

474   Gaussian kernel function, which optimizes the effective dimensionality of the input space

475   (Burges, 1998). We found that our one-versus-all decoding algorithm with the kernel function

476   could not decode orientation above chance when provide with this location information, even

477   though it was given perfect, noise-free information. As a check on the validity of this simulation

478   approach, we also attempted to decode the location of the tip of the teardrop (rather than its

479   orientation) from the X,Y coordinate of the tip, and we found that decoding accuracy was

480   perfect. These simulations show that our decoding algorithm cannot readily decode *orientation*

481   on the basis of the location information even with noise-free data (although it can perfectly

482   decode *location* when given noise-free X,Y coordinates). Consequently, any above-chance

483   decoding of teardrop orientation from the actual EEG data was unlikely to have been based on

484   the location of the thick end of the teardrop.

485   *Cross-Feature Decoding Analyses in Experiment 2*

486   To further demonstrate that orientation can be independently decoded from location, we

487   conducted a cross-feature decoding analysis in which we trained an orientation decoder using

488   trials where the stimulus was presented in the three of the four quadrants of the display and then

489   tested the ability of this decoder to classify orientation in trials were the stimulus was presented

490   in the remaining quadrant (see Fig. 7a). Similarly, we trained a location decoder using trials

491   where the stimulus orientation was in the three of the four quadrants of orientation space and

492   then tested the ability of this decoder to classify location in trials were the stimulus was

493   presented in the remaining set of orientations (see Fig. 7b).

494   For both orientation and location, this decoding was repeated four times (4-fold-cross

495   validation), with each quadrant of the irrelevant feature space serving once as the testing data. As

496   in the main decoding procedure, this procedure was applied to each time point independently.

497   Because the quadrants were fixed rather than random, this procedure was not iterated multiple

498   times (as opposed to the cross-validation procedure used in the main decoding analysis, which

499   was based on random subsets of trials). All other aspects of this procedure were identical to the

500   main decoding procedure.

501   Although the experiment was designed to have equal numbers of trials at each orientation

502   and equal numbers of trials at each tip location, we did not control the number of trials with each

503   orientation-location combination. As a result, the number of trials available for decoding each

504   feature value in the cross-feature decoding procedure varied randomly across iterations, which

505   will tend to reduce the maximum accuracy and reliability of the decoding. Moreover, the cross-

506   feature decoding procedure involved testing the decoder with stimuli that were never used in

507   training, requiring generalization beyond the training set. Thus, if the cross-feature decoding

508   accuracy is above chance, this provides a very stringent test of the ability to decode one

509   dimension with no contribution from the other dimension.

510   Because this was a more stringent test, we performed a statistical analysis that averaged

511   the decoding over all the points during the 1300-ms delay period. We compared the average

512   accuracy during this window to chance using a one-sample *t* test. For the sake of completeness,

513   we also report the accuracy for each individual time point using the same cluster-mass Monte

514   Carlo statistical test used for the main decoding analysis.

515   *Decoding After Excluding Trials with Eye Movements*

516   In our main analyses, we used ICA-based artifact correction to remove the voltage

517   fluctuations produced directly by the eye movements, but this procedure may not correct for

518   other differences in neural activity that may result from sustained changes in eye position. To

519   ensure that the decoding was not based on signals related to eye position, we conducted an

520   additional set of decoding analyses using uncorrected data and excluding trials that could

521   potentially involve systematic shifts in eye position during the delay interval.

522   We first computed the mean HEOG (Right EOG – Left EOG) and VEOG (Lower EOG –

523   Upper EOG) voltages over the delay period, and we subtracted the mean pre-stimulus voltage to

524   correct for the baseline voltage offset. Because systematic eye movements could occur in any

525   direction in this paradigm, it was not sufficient to rely on the individual HEOG and VEOG

526   values. We therefore converted the HEOG and VEOG voltages into a vector (in units of degrees

527   rather than units of µV) representing the angle and amplitude of the eye position relative to the

528   fixation point, using normative scaling values for HEOG (16 µV/°) and VEOG (12 µV/°) (Lins

529   et al., 1993). We then excluded trials from decoding analyses if the amplitude of the eye

530   movement was greater than 0.5425° in any direction (because 0.5425° was half the distance from

531   the fixation dot to the tip location). This very conservative procedure excluded approximately 55%

532   of the trials in Experiment 1 (but many or most of these trials were likely rejected because of

533   noise in the single-trial HEOG and VEOG data, not because of task-related eye movements). The

534   amplitude of the average eye position for a given orientation in the remaining trials was

535   extremely small (0.08°, SEM = 0.01°), indicating that our rejection procedure was successful.

536   We used the same procedure to remove trials with eye movements in Experiment 2, but

537   we used a rejection threshold of 1.085° (because this was half of the distance to the invisible

538   circle that defined the possible locations of the teardrop tip). The exclusion procedure removed

539   approximately 25% of the trials in Experiment 2. The amplitude of the average eye position for a

540   given orientation or location in the remaining trials was again extremely small (0.13°, SEM =

541   0.01°).

542   Excluding trials with eye movements led both to a smaller number of trials and an

543   unequal number of trials for each location and orientation, which would be expected to decrease

544   the reliability of the decoding. Consequently, we focused on average decoding accuracy over the

545   delay period for these analyses.

546   *Code and Data Availability*

547   Both the data and the Matlab analysis scripts are available upon request from G.B.

548   **Results**

549   *Experiment 1 Behavior*

550   Figure 1c summarizes the behavioral data from Experiment 1. On each trial, accuracy was

551   quantified as the angular difference between the orientation of the sample teardrop and the

552   orientation reproduced by the participant. The mean absolute error was quite small (5.40°, SEM

553   = 0.24). We also fit a standard mixture model to characterize the distribution of response errors

554   in terms of response precision and guess rate (Zhang and Luck, 2008). The vast majority of

555   response errors were clustered around 0°, and the mean guess rate was extremely low (0.7%,

556   SEM = 0.2). Mean precision was quite high (kappa = 77.94, SEM = 5.26).

557   *Experiment 1 Scalp Distributions*

558   Our decoding methods rely on differences in the scalp distribution of alpha-band power

559   and sustained ERPs across teardrop orientations, and Figure 2 shows the grand average scalp

560   maps (averaged across the entire delay interval) for each orientation. The alpha-band maps

561   indicate that alpha power over occipital scalp sites was suppressed (relative to the prestimulus

562   period), consistent with prior research demonstrating that alpha-band activity is suppressed over

563   visual cortex during the delay period of working memory tasks (Fukuda et al., 2015; Erickson et

564   al., 2017). The ERP maps show a positive voltage over posterior scalp sites and a negative

565   voltage over anterior scalp sites. This may reflect a combination of posterior P3-like activity and

566   the negative slow wave that is often observed in WM tasks (Ruchkin et al., 1990; Ruchkin et al.,

567   1992).

568   For both the alpha-band activity and the sustained ERPs, subtle differences in scalp

569   distribution can be seen across the 16 teardrop orientations. However, there is no simple pattern

570   in the changes. This may reflect the fact that multiple brain regions exhibit orientation-specific

571   delay activity (Harrison and Tong, 2009), which could produce a complex pattern of activity on

572   the scalp. However, the lack of a simple pattern is not problematic for decoding methods, which

573   can discover regularities in the scalp distributions even if they are complex and subtle. Also, the

574   maps shown in Figure 2 were averaged across participants and time points, potentially obscuring

575   information in the single-participant and single-time point scalp distributions that were used by

576   our decoding procedure.

577   *Experiment 1 Decoding*

578   Figure 3 shows decoding accuracy for Experiment 1, which used a task that could

579   potentially be performed by means of either spatial attention or orientation memory. Decoding

580   accuracy for alpha-band activity began to rise above chance (0.0625 = 1/16) approximately 200

581   ms after the onset of the sample stimulus, peaked around 600 ms, and remained high until just

582   before the end of the delay period. The cluster mass test indicated that the decoding was

583   significantly greater than chance (1 cluster, $p < 10^{-4}$) for the entire 1300-ms delay period (see

584   shaded region in Fig. 3a). When we excluded trials with eye movements (*eye-movement*

585   *rejection*) rather than using ICA to subtract the electro-oculogram signals (*eye-movement*

586   *correction*), the decoding was still significantly greater than chance when averaged across the

587   delay period ($t(15) = 2.8870$, $p = .0113$, one-sample t-test).

588   ERP-based decoding was also significantly above chance during most of the delay period

589   (2 clusters, $p < 10^{-4}$, $p = .015$), even when we used eye-movement rejection instead of correction

590   ($t(15) = 3.6601$, $p = .0022$, one-sample t-test). However, the time course was somewhat different

591   than that for alpha-based decoding. Decoding accuracy was quite high (more than twice the

592   chance level) from approximately 150-400 ms after the onset of the sample teardrop, which

593   likely reflects the N2pc component during the initial processing of the teardrop (Fahrenfort et al.,

594   2017). Decoding then fell, but remained significantly above chance until the final 200-300 ms of

595   the retention interval. It should be noted that sustained ERP activity (but not alpha-band activity)

596   becomes less reliable as time progresses away from the prestimulus baseline period because of

597   slow drifts in the EEG offset (Luck, 2014), and this may explain why the decoding accuracy fell

598   to non-significant levels by the end of the delay period. Alternatively, if the late ERP activity

599   primarily reflects the content of WM rather than spatial attention, then the decline in ERP-based

600   decoding may reflect reliance on spatial attention rather than true orientation memory to perform

601   the task.

602   In either case, the present results demonstrate that our methods can be used to both alpha-

603   band oscillations and sustained ERPs to successfully decode the orientation being held in WM

604   for most of the delay interval. However, this decoding could reflect either sustained spatial

605   attention on the location of the teardrop's tip or bona fide representations of the teardrop's

606   orientation (or a combination of both). Experiment 2 will distinguish between these possibilities.

607   *Experiment 2 Behavior*

608   In Experiment 2, participants performed the same basic task used in Experiment 1, except

609   that the locations of the sample and test teardrops were independently varied (see Fig. 4a). Thus,

610   maintaining attention on the location of the sample teardrop during the delay period could not be

611   used to remember its orientation.

612   Figure 4d summarizes the behavioral data from Experiment 2. The mean absolute error

613   was again quite low (5.40°, SEM = 0.79). When a mixture model was applied, the mean guess

614   rate was extremely low (0.3%, SEM = 0.01) and the mean precision was quite high (kappa =

615   57.82, SEM = 7.05). However, the precision was significantly lower in this experiment than in

616   Experiment 1 (t(30)=2.29, *p* = .029, two-sample t-test). This difference could indicate that

617   location-specific information is useful in maintaining precise orientation representations, leading

618   to poorer memory when this information cannot be used (i.e., when the sample and test stimuli

619   are at different locations). However, it could also reflect other factors, such as poorer sensory

620   acuity at the peripheral locations used in the present experiment.

621   *Experiment 2 Scalp Distributions*

622   Figure 5 shows the grand average scalp topography for each teardrop orientation

623   (averaged across the location of the teardrop) and each teardrop location (averaged across the

624   orientation of the teardrop). As in Experiment 1, the alpha band maps show a suppression of

625   alpha power over posterior scalp sites (relative to the prestimulus period), whereas the ERP maps

626   show a positive voltage over posterior scalp sites and a negative voltage over anterior scalp sites.

627   *Experiment 2 Decoding*

628   We decoded the orientation of the sample teardrop (collapsed across tip locations) using

629   alpha-band activity in one analysis and ERP activity in another analysis. We also decoded the tip

630   location (collapsed across orientations) in a separate pair of analyses. Figure 6 shows decoding

631   accuracy for each of these analyses. Alpha-based decoding for orientation was extremely weak,

632   remaining within .01 of chance accuracy at all time points, and the accuracy did not exceed

633   chance except for a small cluster of significant time points (1 cluster, *p* = .026) at approximately

634   700 ms (see shaded region in Fig. 6a). By contrast, alpha-based decoding of location was well

635   above chance (1 cluster, $p < 10^{-4}$) from the beginning of the delay interval until approximately

636   1000 ms but then fell to chance by the end of the delay interval. Location decoding was

637   significantly more accurate than orientation decoding (1 cluster, $p < 10^{-4}$) from the beginning of

638   the delay period until approximately 1250 ms (see red horizontal bar in Fig. 6c). The same

639   pattern of results was obtained when we used eye-movement rejection instead of correction.

640   Specifically, alpha-based decoding of orientation was near chance ($t(15) = 1.2225$, $p = .2404$,

641   one-sample t-test), but alpha-based decoding of location was greater than chance ($t(15) = 3.2954$,

642    $p = .0049$, one-sample t-test).

643   In contrast to the alpha-based decoding, the ERP-based decoding of orientation was

644   robust and significantly greater than chance (1 cluster, $p < 10^{-4}$) for almost the entire delay

645   period. ERP-based location was also significantly above-chance (1 cluster, $p < 10^{-4}$) for most of

646   the delay period. The ERP-based decoding was significantly more accurate (1 cluster, $p < 10^{-4}$)

647   for location than for orientation for the first ~600 ms of the delay period, but decoding accuracy

648   for location and orientation was similar for the last ~500 ms of the delay period (see Fig. 6d).

649   The same pattern of results was observed when we used eye-movement rejection instead of

650   correction. Specifically, ERP-based decoding was significantly greater than chance for both

651   orientation ($t(15) = 4.03$, $p = .001$, one-sample t-test) and location ($t(15) = 5.4763$, $p < 10^{-4}$, one-

652   sample t-test). These results demonstrate that sustained ERPs contain information about the

653   specific orientation being maintained in WM, but alpha-band oscillations do not.

654   *Experiment 2 Cross-Feature Decoding*

655   As described in the Materials and Methods section, it is unlikely that the above-chance

656   decoding of orientation we observed in this experiment was based on the location of the tip of

657   the teardrop or any other part of the teardrop. To provide a further test of this claim, we

658   conducted an even more stringent test of the location-independence of the orientation decoding,

659   in which the decoder was trained with the data from three of the four quadrants of the display

660   and then tested on the data from the remaining quadrant (see Fig. 7a). In this analysis, the

661   decoder had no opportunity to learn the spatial properties of the orientations used in the test set,

662   providing an even more rigorous test of the location independence of the decoding. Given that

663   this was a more stringent test with decreased statistical power, our main statistical analyses

664   examined decoding accuracy averaged across the entire 1300-ms delay period.

665   As shown in Figure 7c, alpha-based cross-location decoding of orientation was almost

666   exactly at chance (t(15) = 0.25, p = .60, one-sample t-test). We computed the corresponding

667   Bayes factor (Rouder et al., 2009) using the default JZS scaling factor of .707, and we found that

668   the data were 3.8 times more likely to arise from chance decoding than from above-chance

669   decoding. This provides positive support for the hypothesis that orientation cannot be decoded

670   from alpha-band oscillations when a stringent test is used. In contrast, ERP-based cross-location

671   decoding of orientation (Fig. 7d) was significantly above chance (t(15) = 2.99, p = .0046, one-

672   sample t-test). This decoding was greater than chance for all but two of the participants, and the

673   Bayes factor indicated that the data were 5.9 times more likely to arise from above-chance

674   decoding than to arise from chance decoding. Thus, although it may be impossible to completely

675   dissociate location and orientation information, the present analyses provide strong evidence that

676   the sustained ERPs contained location-independent information about orientation.

677   Figure 8 shows decoding accuracy at each individual time point. There was no sign of

678   above-chance alpha-based decoding of orientation at any point during the delay period, whereas

679   ERP-based decoding of orientation was significantly greater than chance for much of the delay

680   period (3 clusters$,$ p = .011, p = .035, $p < 10^{-4}$). These results provide even stronger evidence that

681   sustained ERP activity contains information about the orientation being held in WM,

682   independent of object location, with no evidence of true orientation information in the alpha-

683   band oscillations.

684   For the sake of completeness, we conducted a parallel cross-orientation decoding analysis

685   for location, in which the decoder was trained using three quarters of the orientations and then

686   tested on the other quarter (see Fig. 7b). When averaged over the entire delay period, cross-

687   orientation decoding of location was significantly greater than chance for both alpha-based

688   decoding (t(15) = 3.09, *p* = .0037, one-sample t-test) and ERP-based decoding (t(15) = 5.01, *p* =

689   .00008, one-sample t-test) (see Fig. 7c and 7d). Analyses of each individual time point (Fig. 8)

690   provided evidence of above-chance location decoding across most of the delay period for both

691   ERP-based decoding *(*1 cluster*, p* < 10^{-4}*)* and alpha-based decoding *(*2 clusters*, p* < 10^{-4}, *p* =

692   .026). Thus, as in the previous analyses, the location of the teardrop could be decoded

693   independently of its orientation from both alpha-band activity and sustained ERP activity.

694   Note that the cross-feature decoding was somewhat less accurate than the original

695   decoding for both orientation and location, which presumably reflects the fact that cross-feature

696   decoding requires explicit generalization to stimuli that were not used for training. In addition,

697   the reliability of the decoding may have been decreased by the fact that, unlike the main

698   decoding analyses, we could not iterate over multiple random assignments of stimuli for these

699   analyses. Thus, the lower accuracy in the cross-feature decoding analyses does not imply that the

700   main analyses were contaminated by information from the other dimension.

701   *Confusion Matrices for Experiment 1 and Experiment 2*

702   The main decoding analyses focused on accuracy for exact decoding of location and orientation,

703   averaged across different stimulus values. Here, we provide the confusion matrix for each

704   combination of stimulus value and classification response to provide a more detailed description

705   of the results. Figure 9 shows the probability of a each possible classification response for each

706   possible stimulus value, averaged over the delay interval and over participants. Separate panels

707   are shown for each combination of signal type (alpha or sustained ERP) and decoded feature

708   (orientation in Experiment 1, location in Experiment 2, and orientation in Experiment 2).

709   In Experiment 1, most of the classification responses were clustered around the true target

710   value (the central diagonal) for both the alpha and ERP signals. Interestingly, a given target

711   value in Experiment 1 was occasionally decoded as being 180° away from the true value

712   (indicated by the white diagonal lines). This could reflect the fact that the orientation of an

713   infinite-length line (as opposed to a ray) cannot be distinguished from an orientation that is 180°

714   away. However, this result could also indicate that observers paid attention to the opposite end of

715   the teardrop on some proportion of trials. In addition, these 180° decoding confusions were rare,

716   and participants exhibited no evidence of 180° confusions in their behavioral responses (see Fig.

717   4). In Experiment 2, both the alpha-based and ERP-based decoding of location exhibited a high

718   probability of classification responses at or near the true value, with no obvious evidence of

719   opposite-direction classification responses.

720   The ERP-based decoding of orientation in Experiment 2 showed a broader range of

721   classification responses around the true value than was observed for orientation in Experiment 1

722   or for location in Experiment 2. However, there was still a clear cluster of classification

723   responses around the true orientation value, and no obvious cluster of responses around the

724   opposite orientation. This indicates that the decoding was primarily sensitive to ray orientation

725   (with 360° of unique values) rather than line orientation (with only 180° of unique values). The

726   confusion matrix for alpha-based decoding of orientation in Experiment 2 showed very little

727   structure, consistent with the near-chance orientation decoding accuracy that was obtained for

728   alpha-band activity in the main analyses.

729   **Discussion**

730   Human scalp EEG activity contains both sustained and oscillating activity during the

731   delay period of WM tasks (van Dijk et al., 2010; Perez and Vogel, 2012; Fukuda et al., 2015),

732   possibly reflecting the representation of information across the delay period. However, these

733   signals might instead reflect support processes, such as attentional mechanisms that prevent

734   interference, rather than the actual WM representations (Sauseng et al., 2009; Bonnefond and

735   Jensen, 2012). The ability to decode the feature value being held in WM from a given neural

736   signal provides much stronger evidence that the signal reflects the WM representation (Postle,

737   2016), and the present study therefore sought to determine whether orientation representations in

738   WM could be decoded from scalp EEG activity. Given the close link between sustained ERP

739   activity and WM capacity for objects (Vogel and Machizawa, 2004; Vogel et al., 2005), we

740   predicted that the sustained ERP activity would reflect the features of the objects being

741   maintained in WM. In contrast, given the close relationship between alpha-band activity and

742   spatial attention (Worden et al., 2000; Rihs et al., 2007), we predicted that alpha-band

743   oscillations would primarily reflect the location of the attended object. The results were

744   consistent with these predictions.

745   Experiment 1 demonstrated that orientation information in a WM task could be decoded

746   from the scalp distribution of both alpha-band oscillations and sustained ERP responses.

747   Previous research has found that alpha-band activity can decode the location being maintained in

748   spatial WM (Foster et al., 2016), but this is the first demonstration that sustained ERPs can

749   decode delay-period activity in a WM task. However, it is quite plausible that participants

750   focused their spatial attention on location of the teardrop's tip throughout the delay period as

751   they prepared to reproduce the teardrop's orientation at the end of the trial. As a result, we may

752   have been decoding the direction of spatial attention rather than a WM representation of

753   orientation per se. This is especially plausible for the alpha-band activity, which has a scalp

754   distribution that changes in a fine-grained manner as the location being attended varies (Rihs et

755   al., 2007).

756   *Distinguishing Between Spatial Attention and the Contents of WM*

757   To distinguish between spatial attention and the contents of WM, the task used in

758   Experiment 2 independently varied the location and orientation of the teardrop, and participants

759   were instructed to remember the teardrop's orientation independently of its location. We found

760   that the orientation being held in WM could be decoded from sustained ERP activity throughout

761   the delay period, even though the orientation of the teardrop could not be predicted from its

762   location. In an even more stringent test of location-independent orientation decoding, we found

763   that orientation could be decoded when the decoder was trained with stimuli from one set of

764   locations and tested with stimuli from a different set of locations. Thus, sustained ERP activity

765   contains information about the feature value being held in WM beyond the location of the object.

766   These results dovetail with previous studies showing that sustained ERP activity is closely tied to

767   individual and group differences in WM capacity (Vogel and Machizawa, 2004; Leonard et al.,

768   2012). However, additional research will be needed to determine whether the sustained activity

769   that was responsible for the decoding in the present study is the same as the sustained activity

770   that has been linked to WM capacity in previous research.

771   We also found that ERP activity could be used to decode the location of the teardrop,

772   especially early in the delay interval. This likely reflects, at least in part, the N2pc component

773   (Luck, 2012), which precisely tracks the location of attended objects (Fahrenfort et al., 2017).

774   The location of the teardrop could also be decoded from the scalp distribution of the

775 alpha-band activity, but there was little or no evidence that alpha-band activity could be used to

776 decode the orientation of the stimulus consistently throughout the delay period. Indeed, when we

777 applied the stricter cross-location test of orientation decoding, alpha-based decoding of

778 orientation was very close to chance throughout the delay period. Moreover, the Bayes factor for

779 this analysis provided positive evidence that the data were more consistent with chance-level

780 decoding than with above-chance decoding. These results are consistent with prior evidence that

781 alpha-band activity is closely tied to attention in perceptual tasks (Adrian and Matthews, 1934;

782 Worden et al., 2000; Sauseng et al., 2005) and serves to prevent interference in nonspatial WM

783 tasks (Sauseng et al., 2009; Bonnefond and Jensen, 2012). The decoding methods used here go

784 beyond the previous research, however, providing evidence that the scalp distribution of alpha-

785 band activity contains decodable information about the location of an object but little or no

786 decodable information about the other features of this object. However, it remains quite plausible

787 that alpha-band activity is used to store object locations in WM, even when the task does not

788 explicitly require location memory (Foster et al., 2017).

789   Although we found little or no evidence of orientation information in alpha-band

790 oscillations (or in any other frequency band), this should not be taken to indicate that neural

791 oscillations have no role in object-based WM representations. The present decoding was based

792 on differences in scalp distribution across feature values, and it is possible that scalp EEG

793 oscillations (and LFP oscillations) contain information about feature values in a non-topographic

794 manner (e.g., by means of phase-amplitude coupling – see Sauseng et al., 2009). Because

795 decoding provides important evidence that a neural signal actually reflects WM representations

796 rather than support processes (Postle, 2016), it will be important for future research to determine

797   whether these non-topographic features of scalp EEG oscillations contain information about the

798   feature value being maintained in WM.

799   *Orientation, Space, and Shape*

800   As mentioned earlier, our task required perceiving ray orientation (360° of unique values)

801   rather than line orientation (180° of unique values). Both behavioral performance and location-

802   independent orientation decoding yielded no evidence of 180° confusions, which may indicate

803   that participants were representing shape rather than orientation per se (Zhang and Luck, 2008).

804   However, populations of end-stopped cells in early areas of visual cortex may be able to code ray

805   orientation (Würtz and Lourens, 2000), so it is also possible that the present results reflect

806   relatively low-level representations of orientation.

807   Note that the orientation representations in the present study may actually be conceived

808   as object-centered spatial representations. Interestingly, fMRI-based decoding of orientation in

809   primary visual cortex is not location-specific, and the orientation of a grating presented in one

810   hemifield can be decoded from the pattern of activity in either hemisphere (Ester et al., 2009).

811   This suggests that object-centered representations may involve early visual cortex and not just

812   high-level areas.

813   *Underlying neural activity*

814   Although the present study found that sustained scalp-recorded ERP activity contained

815   information about the orientation value being stored in WM, it is important to ask whether this

816   could be the result of brief bursts of activity that create the appearance of a sustained response

817   when averaged across neurons and/or trials. Our ERP-based decoding was based on data in

818   which activity above 6 Hz was filtered out, so oscillations in the alpha, beta, and gamma bands

819   could not have contributed significantly to the decoding. This includes both the asymmetric

820   alpha oscillations reported by Mazaheri and Jensen (2008) and van Dijk et al. (2010) and the

821   gamma-band LFP bursts observed in monkeys by Lundqvist et al. (2016). However, the gamma

822   bursts were accompanied by single-unit activity that carried information about the stimulus being

823   represented; if these bursts of activity were accompanied by non-oscillating LFPs, the summed

824   activity across a large population of neurons could have created sustained delay-period activity at

825   the scalp. In this way, the sustained ERP-based decoding observed in the present study could

826   reflect infrequent bursts of activity in individual neurons that produced sustained potentials when

827   averaged across cells. In addition, it is possible that WM-related EEG signals were present

828   during some portions of the delay period on some trials and other portions of the delay period on

829   other trials rather than being sustained across the entire delay period on every trial (as has been

830   observed in single-unit activity by Shafi et al., 2007).

831   Nonetheless, the present results put significant constraints on the neural signals that

832   underlie decoding of WM content from scalp EEG signals. For example, the present results

833   unambiguously demonstrate that the EEG contains decodable information about the remembered

834   stimulus value that cannot be directly explained by oscillating LFPs, and they provide no

835   evidence that the scalp distribution of alpha-band oscillations carries information about the

836   contents of WM. Moreover, the present results imply that neural representation of orientation in

837   WM is spatiotopically mapped at a sufficiently coarse cortical scale that it can be decoded even

838   after the substantial spatial filtering that occurs when electrical potentials travel from the neurons

839   that generate them through the brain and skull to the surface of the scalp. However, additional

840   empirical research and modeling will be needed to determine the precise nature of the cellular

841   activity that produces the scalp ERP signals that were decoded in the present study.

842   **References**

843   Adrian ED, Matthews BHC (1934) The Berger rhythm: Potential changes from the occipital
844   lobes in man. Brain 57:355-385.
845   Awh E, Jonides J (2001) Overlapping mechanisms of attention and spatial working memory.
846   Trends in Cognitive Sciences 5:119-126.
847   Awh E, Jonides J, Reuter-Lorenz PA (1998) Rehearsal in spatial working memory. Journal of
848   Experimental Psychology: Human Perception & Performance 24:780-790.
849   Awh E, Anllo-Vento L, Hillyard SA (2000) The role of spatial selective attention in working
850   memory for locations: evidence from event-related potentials. Journal of Cognitive
851   Neuroscience 12:840-847.
852   Bisiach E (1996) Unilateral neglect and the structure of space representation. Current Directions
853   in Psychological Science 5:62-65.
854   Bonnefond M, Jensen O (2012) Alpha oscillations serve to protect working memory
855   maintenance against anticipated distracters. Current biology : CB 22:1969-1974.
856   Brainard DH (1997) The psychophysics toolbox. Spatial Vision 10:433-436.
857   Brouwer GJ, Heeger DJ (2011) Cross-orientation suppression in human visual cortex. Journal of
858   neurophysiology 106:2108-2119.
859   Burges CJ (1998) A tutorial on support vector machines for pattern recognition. Data mining and
860   knowledge discovery 2:121-167.
861   Chun MM, Golomb JD, Turk-Browne NB (2011) A Taxonomy of External and Internal
862   Attention. Annual Review of Psychology 62:73-101.
863   Delorme A, Makeig S (2004) EEGLAB: an open source toolbox for analysis of single-trial EEG
864   dynamics including independent component analysis. Journal of Neuroscience Methods
865   134:9-21.
866   Dietterich TG, Bakiri G (1995) Solving multiclass learning problems via error-correcting output
867   codes. Journal of artificial intelligence research 2:263-286.
868   Drisdelle BL, Aubin S, Jolicoeur P (2017) Dealing with ocular artifacts on lateralized ERPs in
869   studies of visual-spatial attention and memory: ICA correction versus epoch rejection.
870   Psychophysiology 54:83-99.
871   Erickson MA, Albrecht MA, Robinson BM, Luck SJ, Gold JM (2017) Impaired suppression of
872   delay-period alpha and beta is associated with impaired working memory in
873   schizophrenia   Biological Psychiatry: Cognitive Neuroscience and Neuroimaging 2:272-
874   279.
875   Ester EF, Serences JT, Awh E (2009) Spatially global representations in human primary visual
876   cortex during working memory maintenance. Journal of Neuroscience 29:15258-15265.
877   Ester EF, Anderson DE, Serences JT, Awh E (2013) A neural measure of precision in visual
878   working memory. Journal of Cognitive Neuroscience 25:754-761.
879   Ester EF, Drew T, Klee D, Vogel EK, Awh E (2012) Neural measures reveal a fixed item limit in
880   subitizing. Journal of Neuroscience 32:7169-7177.
881   Fahrenfort JJ, Grubert A, Olivers CN, Eimer M (2017) Multivariate EEG analyses support high-
882   resolution tracking of feature-based attentional selection. Scientific reports 7:1886.
883   Foster JJ, Bsales EM, Jaffe RJ, Awh E (2017) Alpha-Band Activity Reveals Spontaneous
884   Representations of Spatial Position in Visual Working Memory. Current biology : CB
885   27:3216-3223.

886   Foster JJ, Sutterer DW, Serences JT, Vogel EK, Awh E (2016) The topography of alpha-band
887   activity tracks the content of spatial working memory. Journal of neurophysiology
888   115:168-177.
889   Foster JJ, Sutterer DW, Serences JT, Vogel EK, Awh E (in press) Alpha-Band Oscillations
890   Enable Spatially and Temporally Resolved Tracking of Covert Spatial Attention.
891   Psychological Science.
892   Fukuda K, Mance I, Vogel EK (2015) α power modulation and event-related slow wave
893   provide dissociable correlates of visual working memory. Journal of Neuroscience
894   35:14009-14016.
895   Gazzaley A, Nobre AC (2012) Top-down modulation: bridging selective attention and working
896   memory. Trends in Cognitive Sciences 16:129-135.
897   Groppe DM, Urbach TP, Kutas M (2011) Mass univariate analysis of event-related brain
898   potentials/fields I: a critical tutorial review. Psychophysiology 48:1711-1725.
899   Harrison SA, Tong F (2009) Decoding reveals the contents of visual working memory in early
900   visual areas. Nature 458:632-635.
901   Johnson JS, Hollingworth A, Luck SJ (2008) The role of attention in the maintenance of feature
902   bindings in visual short-term memory. Journal of Experimental Psychology: Human
903   Perception and Performance 34:41-55.
904   Jolicoeur P, Brisson B, Robitaille N (2008) Dissociation of the N2pc and sustained posterior
905   contralateral negativity in a choice response task. Brain research 1215:160-172.
906   Jung TP, Makeig S, Westerfield M, Townsend J, Courchesne E, Sejnowski TJ (2000) Removal
907   of eye activity artifacts from visual event-related potentials in normal and clinical
908   subjects. Clinical Neurophysiology 111:1745-1758.
909   LaRocque JJ, Lewis-Peacock JA, Drysdale AT, Oberauer K, Postle BR (2013) Decoding
910   attended information in short-term memory: an EEG study. Journal of Cognitive
911   Neuroscience 25:127-142.
912   Leonard CJ, Kaiser ST, Robinson BM, Kappenman ES, Hahn B, Gold JM, Luck SJ (2012)
913   Toward the neural mechanisms of reduced working memory capacity in schizophrenia.
914   Cerebral Cortex 23:1582-1592.
915   Lins OG, Picton TW, Berg P, Scherg M (1993) Ocular artifacts in EEG and event-related
916   potentials I: Scalp topography. Brain Topography 6:51-63.
917   Lopez-Calderon J, Luck SJ (2014) ERPLAB: An open-source toolbox for the analysis of event-
918   related potentials. Front Hum Neurosci 8:213.
919   Luck SJ (2012) Electrophysiological correlates of the focusing of attention within complex
920   visual scenes: N2pc and related ERP components. In: The Oxford Handbook of ERP
921   Components (Luck SJ, Kappenman ES, eds), pp 329-360. New York: Oxford University
922   Press.
923   Luck SJ (2014) An Introduction to the Event-Related Potential Technique, Second Edition.
924   Cambridge, MA: MIT Press.
925   Lundqvist M, Rose J, Herman P, Brincat SL, Buschman TJ, Miller EK (2016) Gamma and beta
926   bursts underlie working memory. Neuron 90:152-164.
927   Maris E, Oostenveld R (2007) Nonparametric statistical testing of EEG- and MEG-data. Journal
928   of Neuroscience Methods 164:177-190.
929   Mazaheri A, Jensen O (2008) Asymmetric amplitude modulations of brain oscillations generate
930   slow evoked responses. Journal of Neuroscience 28:7781-7787.

931 Miller EK, Desimone R (1991) A neural mechanism for working and recognition memory in
932   inferior temporal cortex. Science 254:1377-1379.
933 Pelli DG (1997) The VideoToolbox software for visual psychophysics: Transforming numbers
934   into movies. Spatial Vision 10:437-442.
935 Perez VB, Vogel EK (2012) What ERPs can tell us about working memory. In: The Oxford
936   Handbook of Event-Related Potential Components (Luck SJ, Kappenman ES, eds), pp
937   361-372. New York: Oxford University Press.
938 Postle BR (2016) How does the brain keep information "in mind"? Current Directions in
939   Psychological Science 25:151-156.
940 Rihs TA, Michel CM, Thut G (2007) Mechanisms of selective inhibition in visual spatial
941   attention are indexed by α-band EEG synchronization. The European journal of
942   neuroscience 25:603-610.
943 Rose NS, LaRocque JJ, Riggall AC, Gosseries O, Starrett MJ, Meyering EE, Postle BR (2016)
944   Reactivation of latent working memories with transcranial magnetic stimulation. Science
945   354:1136-1139.
946 Rouder JN, Speckman PL, Sun D, Morey RD, Iverson G (2009) Bayesian t tests for accepting
947   and rejecting the null hypothesis. Psychonomic Bulletin & Review 16:225-237.
948 Ruchkin DS, Johnson R, Jr., Canoune H, Ritter W (1990) Short-term memory storage and
949   retention: an event-related brain potential study. Electroencephalography and clinical
950   neurophysiology 76:419-439.
951 Ruchkin DS, Johnson R, Jr., Grafman J, Canoune H, Ritter W (1992) Distinctions and
952   similarities among working memory processes: an event-related potential study. Brain
953   Research: Cognitive Brain Research 1:53-66.
954 Sauseng P, Klimesch W, Stadler W, Schabus M, Doppelmayr M, Hanslmayr S, Gruber WR,
955   Birbaumer N (2005) A shift of visual spatial attention is selectively associated with
956   human EEG alpha activity. The European journal of neuroscience 22:2917-2926.
957 Sauseng P, Klimesch W, Heise KF, Gruber WR, Holz E, Karim AA, Glennon M, Gerloff C,
958   Birbaumer N, Hummel FC (2009) Brain oscillatory substrates of visual short-term
959   memory capacity. Current biology : CB 19:1846-1852.
960 Serences JT, Ester EF, Vogel EK, Awh E (2009) Stimulus-specific delay activity in human
961   primary visual cortex. Psychological Science 20:207-214.
962 Shafi M, Zhou Y, Quintana J, Chow C, Fuster J, Bodner M (2007) Variability in neuronal
963   activity in primate cortex during working memory tasks. Neuroscience 146:1082-1108.
964 Stokes MG (2015) 'Activity-silent' working memory in prefrontal cortex: a dynamic coding
965   framework. Trends in Cognitive Sciences 19:394-405.
966 Tas AC, Luck SJ, Hollingworth A (2016) The Relationship between Visual Attention and Visual
967   Working Memory Encoding: A Dissociation between Covert and Overt Orienting.
968   Journal of Experimental Psychology: Human Perception and Performance 42:1121-1138.
969 Todd JJ, Marois R (2004) Capacity limit of visual short-term memory in human posterior
970   parietal cortex. Nature 428:751-754.
971 van Dijk H, van der Werf J, Mazaheri A, Medendorp WP, Jensen O (2010) Modulations in
972   oscillatory activity with amplitude asymmetry can produce cognitively relevant event-
973   related responses. Proceedings of the National Academy of Sciences 107:900–905.

974   van Ede F, Niklaus M, Nobre AC (2017) Temporal expectations guide dynamic prioritization in
975   visual working memory through attenuated α oscillations. Journal of Neuroscience
976   37:437-445.
977   Vogel EK, Machizawa MG (2004) Neural activity predicts individual differences in visual
978   working memory capacity. Nature 428:748-751.
979   Vogel EK, McCollough AW, Machizawa MG (2005) Neural measures reveal individual
980   differences in controlling access to working memory. Nature 438:500-503.
981   Wolff MJ, Ding J, Myers NE, Stokes MG (2015) Revealing hidden states in visual working
982   memory using electroencephalography. Frontiers in systems neuroscience 9.
983   Wolff MJ, Jochim J, Akyürek EG, Stokes MG (2017) Dynamic hidden states underlying
984   working-memory-guided behavior. Nature Neuroscience 20:864-871.
985   Woodman GF, Vogel EK, Luck SJ (2001) Visual search remains efficient when visual working
986   memory is full. Psychological Science 12:219-224.
987   Worden MS, Foxe JJ, Wang N, Simpson GV (2000) Anticipatory biasing of visuospatial
988   attention indexed by retinotopically specific alpha-band electroencephalography
989   increases over occipital cortex. Journal of Neuroscience 20:RC63.
990   Würtz RP, Lourens T (2000) Corner detection in color images through a multiscale combination
991   of end-stopped cortical cells. Image and Vision Computing 18:531-541.
992   Zhang W, Luck SJ (2008) Discrete fixed-resolution representations in visual working memory.
993   Nature 453:233-235.
994

995

996   Figure 1. (a) Possible attention-based strategy for remembering an orientation. Maintaining
997   attention on one or both of the extreme ends of the grating over a delay interval could help an
998   observer reproduce the orientation or detect changes in orientation at the end of the interval.
999   Even if this was not the sole mechanism being used for the task, it would likely be useful for
1000 performing the task, and neural signals related to spatial attention could potentially be sufficient
1001 to produce above-chance decoding of the orientation. (b) Delayed estimation task used in
1002 Experiment 1. On each trial, participants fixated at the central dot for 500 ms (not shown here)
1003 and then saw a 200-ms teardrop. After a 1300-ms delay period, a response ring appeared,
1004 followed by a test teardrop as soon as the participant began moving the mouse. Participants used
1005 the mouse to adjust the orientation of the test teardrop until it matched the remembered
1006 orientation of the sample teardrop. The tip of the test teardrop pointed toward the mouse cursor,
1007 and participants clicked the mouse button to finalize their report. (c) Probability distribution of
1008 response errors in Experiment 1, collapsed across all participants.
1009
1010
1011 Figure 2. Topography of (a) instantaneous alpha power and (b) ERP activity for each of 16
1012 sample orientations, averaged across the delay interval and participants in Experiment 1. Both
1013 alpha power and ERP amplitude were computed relative to the prestimulus baseline period. The
1014 position of each scalp map corresponds to the orientation of the sample teardrop.
1015
1016
1017 Figure 3. Mean accuracy of (a) alpha-based decoding and (b) ERP-based decoding in Experiment
1018 1. Chance-level performance ($0.0625 = 1/16$) is indicated by the black horizontal lines. Gray
1019 areas indicate clusters of time points in which the decoding was significantly greater than chance
1020 after correction for multiple comparisons. Note that the first 200 ms following stimulus onset
1021 were excluded from the statistical analysis to minimize any contributions of sensory activity to
1022 the decoding. The orange shading indicates ± 1 SEM.
1023
1024
1025 Figure 4. (a) Two example trials of the delayed estimation used in Experiment 2: On each trial,
1026 participants fixated the central dot for 500 ms (not shown here) and then saw a 200-ms teardrop.
1027 After a 1300-ms delay period, a second teardrop was presented at a different random location,
1028 and the participant used a mouse to adjust this second teardrop's orientation so that it matched
1029 the remembered orientation of the first teardrop. (b) Definition of θ_L (the angular location of the
1030 teardrop tip) and θ_O (the orientation of the teardrop): θ_L was defined by the location (in polar
1031 coordinates) of the tip of the teardrop object relative to an invisible circle with a radius of 2.17°,
1032 centered on the fixation dot. θ_O was defined by the orientation of the tip of the teardrop relative
1033 to the center of the teardrop. (c) Independence of θ_L and θ_O. The tip of a teardrop with a given θ_O
1034 could be presented at any of the 16 θ_L values, and a teardrop with a given θ_L could have any of
1035 the 16 θ_O values. (d) Probability distribution of response errors collapsed across all participants.
1036
1037
1038 Figure 5. Scalp topography of (a) instantaneous alpha power and (b) ERP activity relative to
1039 prestimulus baseline for each of the 16 orientations of the sample teardrop, averaged across the
1040 delay interval and participants. The position of each scalp map corresponds to the orientation of
1041 the sample teardrop. Topography of (c) alpha power and (d) ERP activity for each of the 16

1042   locations of the sample teardrop tip, averaged across the delay interval and participants. The
1043   position of each scalp map corresponds to the location of the tip of the sample teardrop. Both
1044   alpha power and ERP amplitude were computed relative to the prestimulus baseline period.
1045   Figure 6. Alpha-based decoding accuracy for (a) the orientation of the sample teardrop and (c)
1046   the location of the sample teardrop tip. ERP-based decoding accuracy for (b) the orientation of
1047   the sample teardrop and (d) the location of the sample teardrop tip. Each gray area shows a
1048   cluster of time points for which the decoding was greater than chance after correction for
1049   multiple comparisons. The red lines in (c) and (d) indicates clusters of time points in which the
1050   decoding was significantly greater for location than for orientation. The orange shading indicates
1051   ±1 SEM. Note that the first 200 ms following stimulus onset were excluded from the statistical
1052   analysis to minimize any contributions of sensory activity to the decoding.
1053
1054
1055   Figure 7. Cross-feature decoding. (a) To completely remove the impact of the tip location on the
1056   decoding of orientation, we trained the decoders using data from teardrops presented in 3 of the 4
1057   quadrants (indicated by pink locations) and then tested the decoding on trials from the remaining
1058   quadrant (indicated by green locations). This was repeated four times, using each quadrant as the
1059   test quadrant once. (b) The analogous procedure was used for location decoding. The decoders
1060   were trained to decode location using ¾ of the orientations (indicated by pink teardrops), and
1061   then tested with the other ¼ (indicated by green teardrops). (c) Alpha-based cross-feature
1062   decoding accuracy for orientation and location, averaged over the entire delay period (d) ERP-
1063   based cross-feature decoding accuracy for orientation and location, averaged over the entire
1064   delay period for orientation and location. Each participant is represented by a dot, and the mean
1065   and ±1 SEM are indicated by the line and box. ** = $p < .01$, *** = $p < .001$
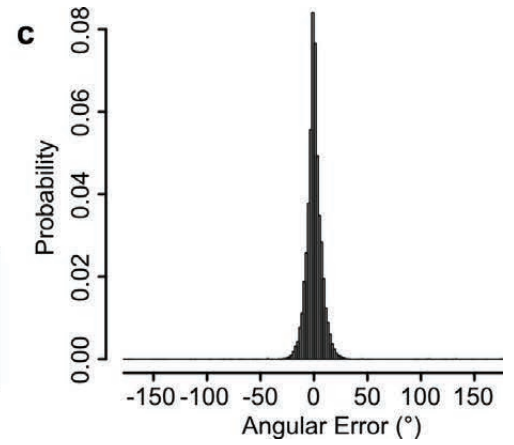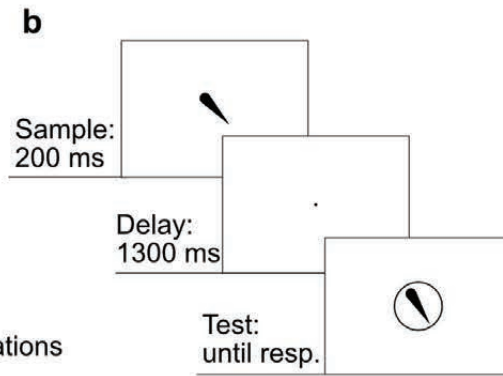1066
1067
1068   Figure 8. Average cross-feature decoding accuracy at each time point. (a) Average accuracy of
1069   alpha-based cross-location decoding of orientation. (b) Average accuracy of ERP-based cross-
1070   location decoding of orientation. (c) Average accuracy of alpha-based cross-orientation decoding
1071   of location. (d) Average accuracy of ERP-based cross-orientation decoding of location. The
1072   orange shading indicates ±1 SEM. Gray areas represent clusters of points with significantly
1073   above-chance decoding accuracy after correction for multiple comparisons. Note that the first
1074   200 ms following stimulus onset were excluded from the statistical analysis to minimize any
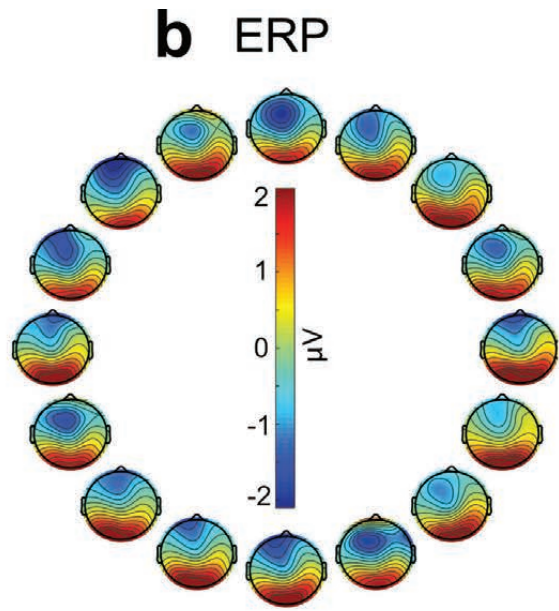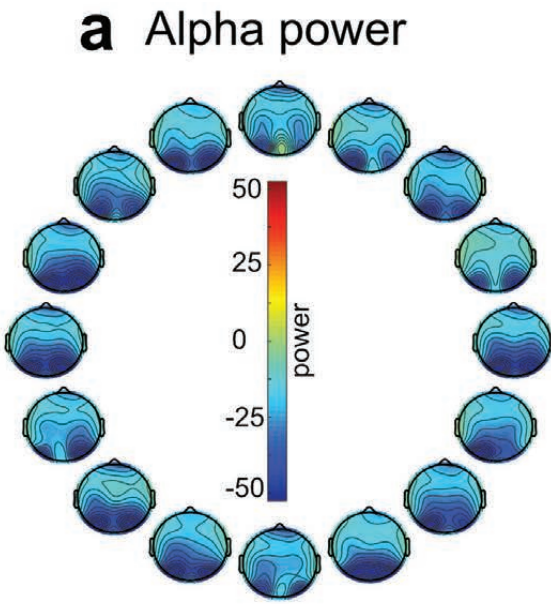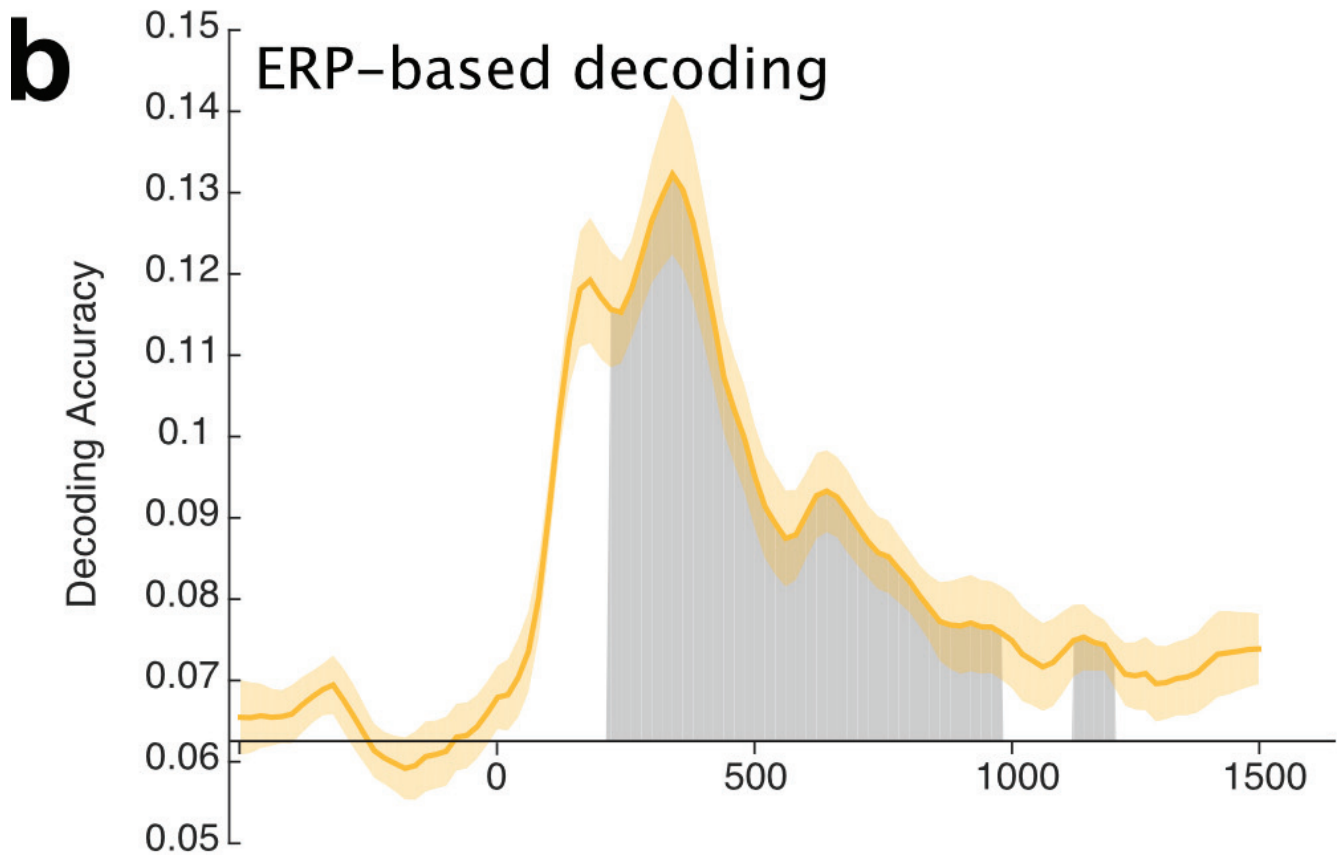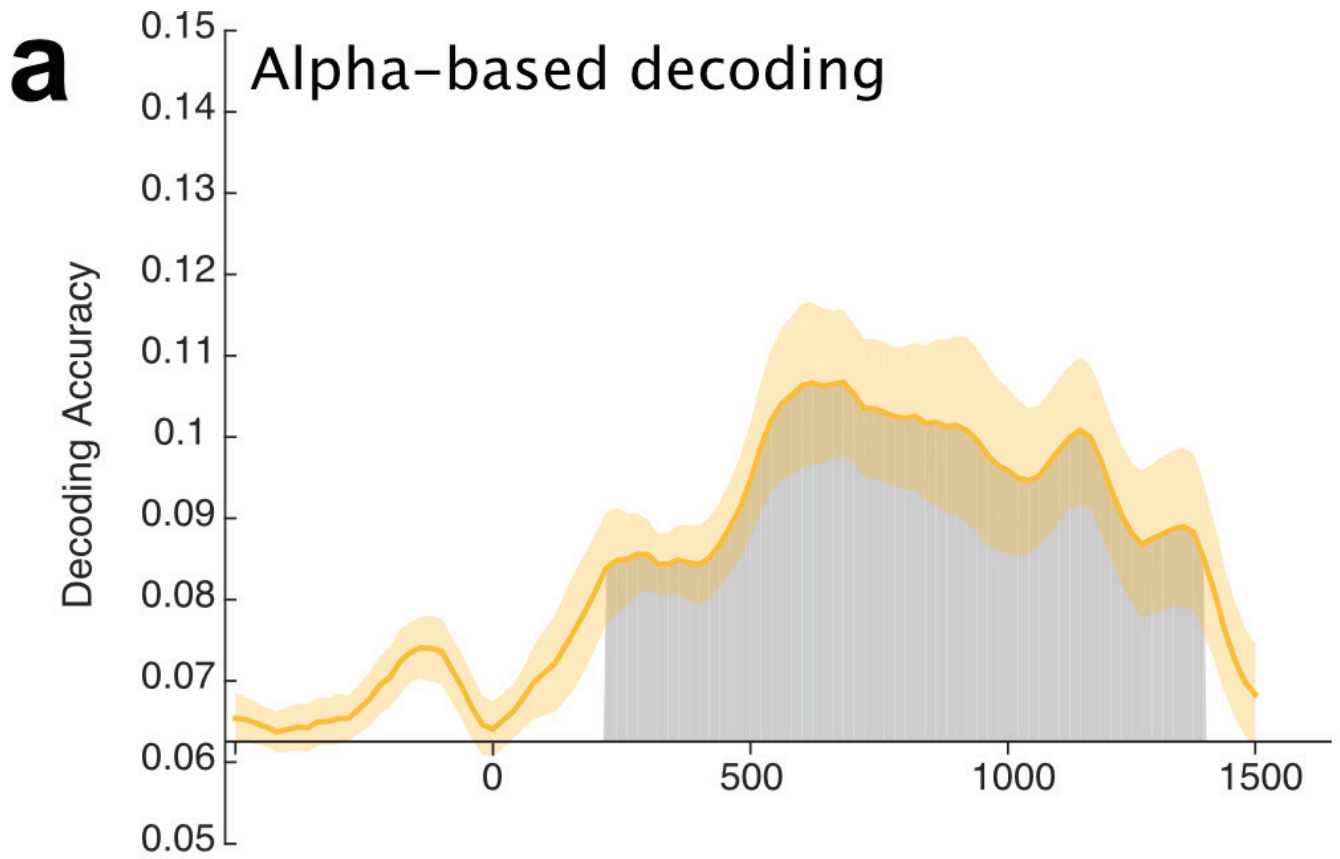1075   contributions of sensory activity to the decoding.
1076
1077
1078   Figure 9. Confusion matrices for alpha-based (top row) and ERP-based (bottom row) decoding
1079   for Experiment 1 (left column), Experiment 2 location (middle column), and Experiment 2
1080   orientation (right column). Each cell shows the probability of a given classification response (X
1081   axis) for given a stimulus value (Y axis), averaged over the entire delay interval and across
1082   observers. The white diagonal lines indicate classification responses that are 180° from the
1083   stimulus value. Note that the values in the upper left and lower right corners of each matrix
1084   represent stimulus-response combinations that are actually adjacent to the stimulus-response
1085   combinations in the lower left and upper right corners (because these matrices provide a linear
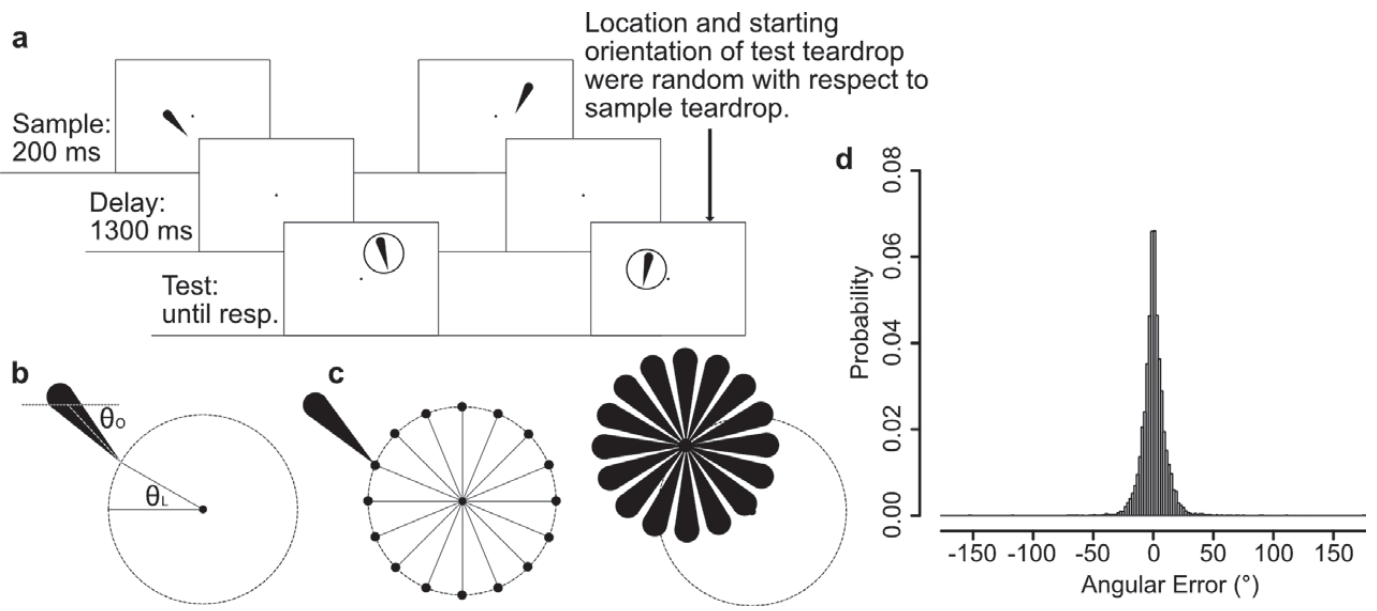1086   representation of a circular stimulus space).

a
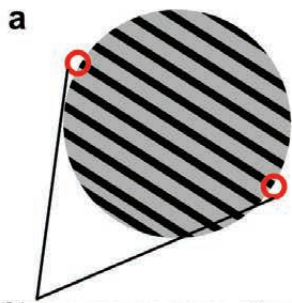
Observers can pay attention
to either or both of these locations
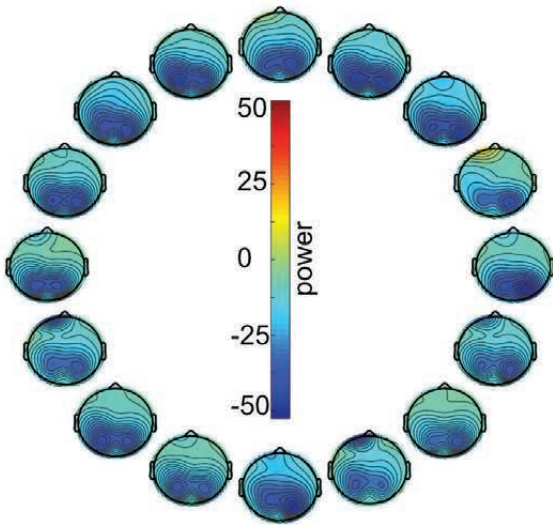to remember the orientation
of the grating.

b

Sample:
200 ms

Delay:
1300 ms

Test:
until resp.

c

a Alpha power

b ERP

a Alpha-based decoding

b ERP-based decoding

a

Sample:
200 ms

Delay:
1300 ms

Test:
until resp.

Location and starting
orientation of test teardrop
were random with respect to
sample teardrop.

b

θ_O

θ_L

c

d

Probability
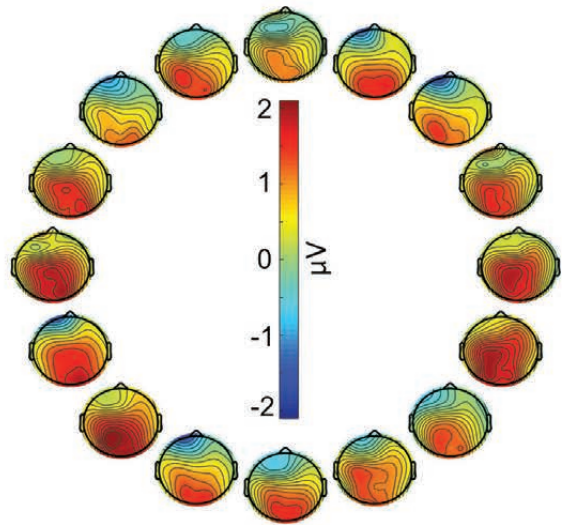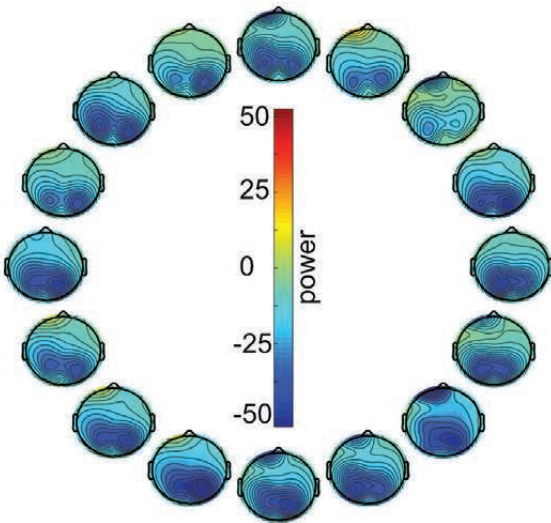
Angular Error (°)

a Alpha power: Orientation

b ERP: Orientation

c Alpha power: Location

d ERP: Location

a Alpha-based decoding: Orientation

b ERP-based decoding: Orientation

c Alpha-based decoding: Location

d ERP-based decoding: Location

a

b

c Alpha-based
cross-feature decoding

d ERP-based
cross-feature decoding

a Alpha-based cross-location decoding: Orientation

b ERP-based cross-location decoding Orientation

c Alpha-based cross-orientation decoding: Location

d ERP-based cross-orientation decoding: Location